World Academy of Science, Engineering and Technology
International Journal of Biomedical and Biological Engineering
Vol:18, No:7, 2024

Electrodermal Activity Measurement Using Constant Current AC Source

Cristian Chacha, David Asiain, Jesús Ponce de León, José Ramón Beltrán

***Abstract*—**This work explores and characterizes the behavior of the AFE AD5941 in impedance measurement using an embedded algorithm that allows using a constant current AC source. The main aim of this research is to improve the exact measurement of impedance values for their application in EDA-focused wearable devices. Through comprehensive study and characterization, it has been observed that employing a measurement sequence with a constant current source produces results with increased dispersion but higher accuracy and a more linear behavior with respect to error. As a result, this approach leads to a more accurate system for impedance measurement.

***Keywords*—**Electrodermal Activity, constant current AC source, wearable, precision, accuracy, impedance.

I. Introduction

THE study of emotional intelligence has been present during the last decades, showing itself as the key point in improving the quality of life. Numerous studies have shown that the state of mind and the management of emotions are directly related to the physical conditions a person may present and the effectiveness while performing activities [1], [2], as well as improvements in various areas of daily life. According to [3], the first step to acquiring greater awareness about emotional intelligence and the management of our emotions is perception.

Several investigations on electrodermal activity (EDA) [4]-[7] show a high correlation between skin impedance values and stress levels, as well as other emotions such as fear, anxiety and various cognitive states. This correlation persists even when we are asleep. Therefore, the measurement of EDA has many advantages in recording, analyzing, and recognizing emotional states.

Skin impedance is related to the behavior of the parasympathetic system [8], [9] demonstrating correlation between skin impedance and the behavior of the parasympathetic system. These resources emphasize that this is a system over which we have no conscious control and is in turn related to various organs of the body, including the skin and specifically the sweat glands.

EDA opens up the possibility of measuring changes in skin conductivity or impedance without the use of intrusive methods, which has led to the development of wearable devices [10]-[14], although currently many of these devices only make use of DC voltage methods.

II. Electrodermal Activity

EDA is the study of the characteristics present in the electrical signals produced by manifestations of the parasympathetic system, which is innervated by sweat glands [15]. This way, changes in the parasympathetic system create greater activity in the sweat glands present in the skin, which in turn generate sweat. The composition of swear is mainly NaCl [9], so the dermis and epidermis exhibit a varying level of resistance to current flow. This, in turn, indicates a change in skin impedance.

Different layers of the skin can be modeled using passive electrical components such as resistors and capacitors. However, this model may vary depending on the measurement methods and the interface used between the skin and the electronic device used for measurement [16]. Fig. 1 presents a comprehensive model of the skin and the dry/wet electrode interface.

Fig. 1 represents the electrical model of the skin, it considers the epidermis and dermis layer as most important part; we note that the subscript *ep* refers to the epidermis, while the subscript *sw* is related to the activity of sweat glands pertaining to sweat related to the activity of sweat glands [16]. The electrical model of the epidermis and sweat parts consists of the parallel of a resistance and a capacitance, in series with a voltage source. The passive components can be considered as an equivalent impedance. The variation of resistance (R_{SW}) is related to sweat gland activity. The variation of C_{SW} is also induced by sweat, since sweat, in the sweat gland ducts, acts as the dielectric of a capacitor. The values of C_{EP}, R_{EP}, and R_d (dermis resistance) are different for each user but show a low fluctuation [8].

Exosomatic EDA measurements can be carried out using DC and AC excitation voltages. The presence of the reactance component is achieved only when using an AC measurement technique. This is because the DC current does not produce any further disturbances once the capacitors are charged. In addition, the AC current source technique avoids electrode polarization, since the current flow is altered at each oscillation cycle. Therefore, the use of an AC source has at least two obvious advantages: it allows the use of dry electrodes and provides more information about changes in skin impedance.

III. EDA Device

To measure skin impedance, Analog Devices AD-5941 are used. This is a smart Analog-Front-End (AFE) device, whose

Cristian Chacha, David Asiain, Jesus Ponce de León, and José Ramón Beltran are with Department of Electronics, Escuela Universitaria Politécnica de La Almunia, La Almunia de Doña Godina, 50100 Zaragoza, Spain (e-mail: cristianchachaleon@gmail.es, dasiain@unizar.es, jponce@unizar.es, jrbelbla@unizar.es).

accuracy and precision will be characterized. The AD-5941 is a complete data acquisition system packaged in a 7 mm × 7 mm, 48-lead LFCSP. This device is responsible for generating an AC signal between two electrodes, measuring the voltage difference (V_{exc}) and the current value (I) across these two points. With these two measures, the impedance can be calculated using (1) is used. In this equation, all involved values can have real and imaginary part.

$$Z_{UKNOWN} = \frac{V_{exc}}{I} - R_{LIMIT} - \frac{1}{2 \cdot 100 \cdot \pi}\left(\frac{1}{c_{ISO1}} + \frac{1}{c_{ISO2}}\right) \quad (1)$$

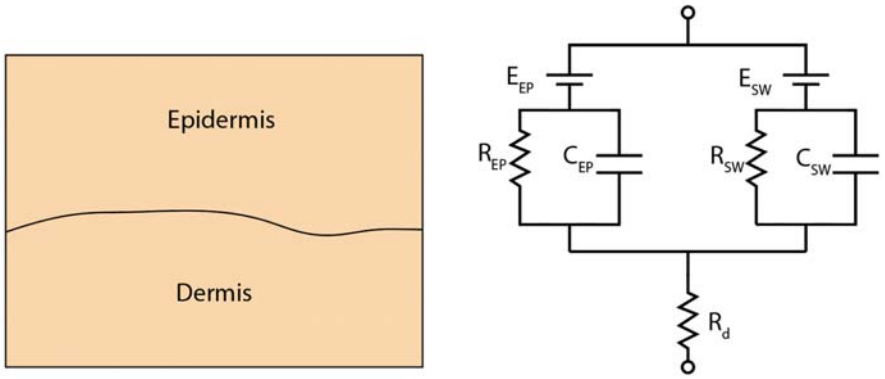

Fig. 1 Electrical model of the skin impedance

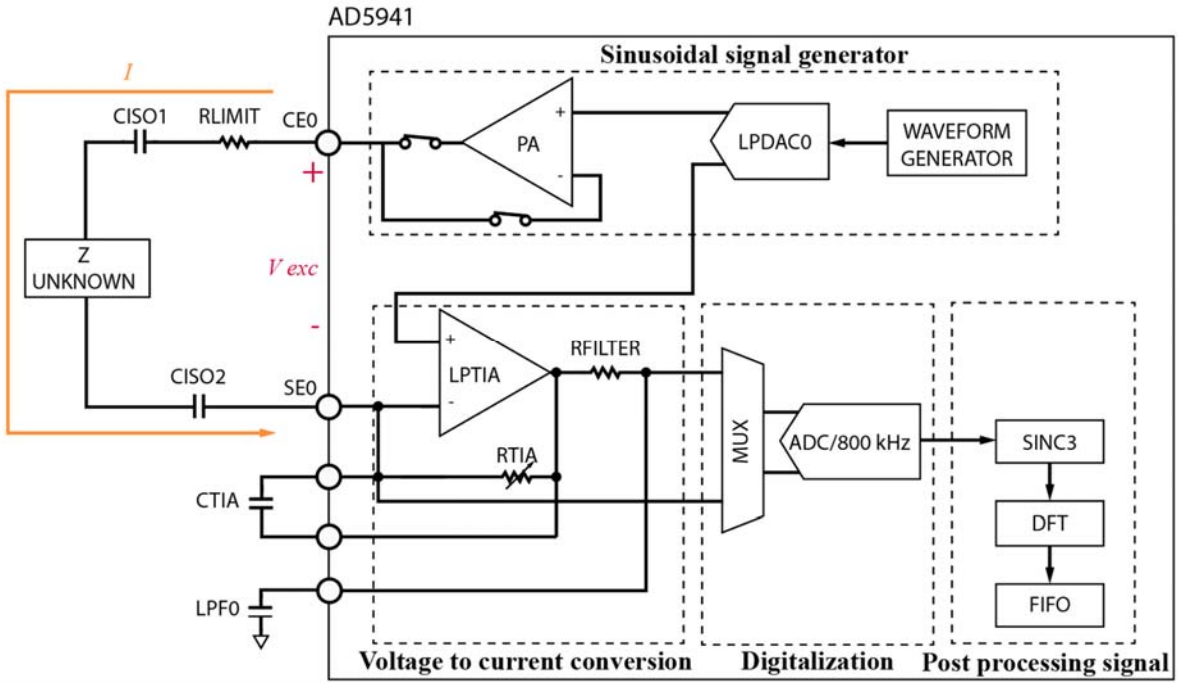

Fig. 2 Measurement of impedance using the AD-5941 IC

Fig. 2 shows a high-level vision of modules inside of the AD-5941. Four main parts can be distinguished: the sinusoidal signal generator, a current-to-voltage conversion, an ADC, and the post-processing of the signal.

The first stage incorporates a digital waveform generator which uses a low-power digital-to-analog converter (LPDAC). The LPDAC has two outputs: one with a 12-bit resolution, which is used to generate a sinusoidal waveform with an offset voltage, and the second output with a 6-bit resolution, which generates the offset voltage for the current-to-voltage converter stage.

The waveform generated by the LPDAC has a maximum range value of 0.2-2.4V. To maintain the voltage value, a potentiostat (PA) is employed. The sinusoidal waveform V_{exc}, generated between the CE0 and SE0 pins, has a frequency of 100 Hz and an amplitude of 0.9 V without offset. Additionally, the system incorporates two capacitors to prevent direct current from flowing through the skin, in compliance with the IEC 60601 standard [17].

A capital part of this study focuses on the current to voltage converter stage. This conversion is done through a low power transimpedance amplifier (LPTIA). To perform this conversion, the LPTIA requires a feedback resistor (RTIA), which value is selected by the Micro Controller Unit (MCU)

based on input current. Since this current can vary from 50 pA to 3 mA [18], the AD-5941 features a RTIA range from 1 kΩ to 512 kΩ.

The selected value of RTIA is in parallel with a capacitor to reduce oscillation in the current-to-voltage conversion. Therefore, the feedback impedance and the entire set of resistors must be calibrated at the beginning of the measurement.

The digitalization stage uses an ADC capable of 800 kilo-samples per second. The use of a high sampling frequency is beneficial for the post-processing stage of the signal. The matrix configuration of the device allows using different inputs for the ADC, such as PA or LPTIA allowing for the measurement of voltage generated and current flowing through $Z_{UNKNOWN}$.

The use of such a high sampling frequency has advantages for the post-processing stage of the signal. In this last stage, a digital filter (SINC3) and a discrete Fourier transform (DFT) are used. This enables a frequency sweeping and the selection of magnitude and phase values for specific frequencies from the waveform generator in the first stage. The final step involves saving the information in a FIFO memory and transmitting voltage and current values, both in magnitude and phase, to the microcontroller using SPI communication.

It is worth mentioning that the AD-5941 features a programmable sequencer that allows for the execution of all measurement steps independently. This sequence needs to be programmed initially and it can also be modified in real-time by the microcontroller.

IV. Measurement of Impedance

This section describes the implementation of the sequence used to perform an impedance measurement using a constant current source without the need to add other external hardware components to achieve it.

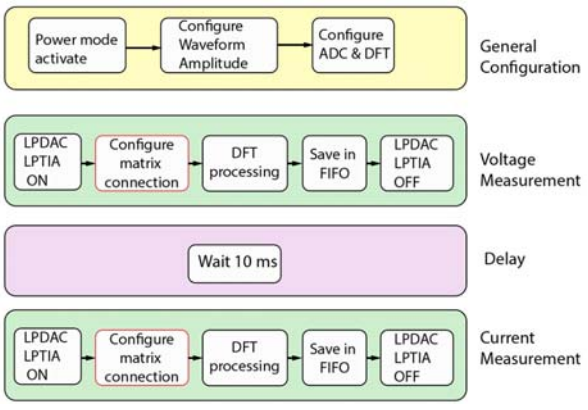

Fig. 3 Sequence load in AFE AD-5941

The main idea of this measurement method is to use the waveform generator as a generator of sinusoidal signals, with a variable amplitude but maintaining a frequency of 100 Hz. This generator operates within a limited range of voltage values. Fig. 3 shows the complete sequence that the MCU loads into the AD-5941. This sequence is executed automatically every 250 ms, without MCU intervention, as will be detailed later.

As can be seen in Fig. 3, the first stage in the sequence is to configure all modules of the AD-5941 and switch to active power mode. In this step, the waveform is configured with a specific amplitude value for the sinusoidal signal. This first stage only involves configuration and does not power on any module.

The next stage involves the voltage measurement. The LPDAC and LPTIA modules are switched on and the matrix connection is configured to measure the voltage value of the PA (connected to the LPDAC). Additionally, the DFT processing signal is performed and saved in the FIFO. After this voltage measurement, the device switches off the modules and does not generate any voltage signal. In this stage, output voltage is not present in CE0 pin (blue path in Fig. 4), therefore there is not current flow in the $Z_{UNKNOWN}$ impedance.

There is a stage delay of 10 ms to achieve signal stabilization and discharge the passive components, thus avoiding erroneous measurements.

The current measurement stage is very similar to the voltage stage. The steps are the same, except for the configuration of the matrix connection, which allows us to connect the output of the PA to the CE0 pin and inject current through Z_{UKNOWN}.

LPTIA is configured to has current input from pin SE0. Fig. 4 illustrates difference between connection to voltage measurement (blue path) and current measurement (orange path).

Taking into account that the value of the $Z_{UNKNOWN}$ impedance (and therefore the current flowing through it) can vary, a feedback current value is calculated, and a voltage amplitude adjustment is made. This adjustment is intended to ensure that the current flowing through $Z_{UNKNOWN}$ remains constant and is within a value close to but not exceeding 10 uA, in compliance with IEC 60601. Since the current range remains constant, the need to change or calibrate other feedback impedance values in the LPTIA is eliminated, so a single value of the RTIA feedback resistor is used.

A complete illustration of the sequence execution can be seen in Fig. 5. During the device initialization, the voltage signal has an amplitude of 1 mV. After four measurements and communication with the MCU, the embedded sequence is modified to generate a new amplitude in the sinusoidal signal.

As can be seen in Fig. 5, a voltage measurement is performed before each current measurement, unlike the algorithm proposed by Analog Devices, where a voltage measurement is only realized at the beginning of the sequence under the assumption that the value remains constant. This approach adds significant value to the measurement process as voltage and current samples are taken in each sample. Considering that the device may be subjected to environmental changes, a quasi-simultaneous measurement of voltage and current is achieved, resulting in a more accurate impedance measurement value.

During the development of the algorithm, it was observed that conducting multiple consecutive measurements of the applied voltage resulted in a high dispersion of these values, with a deviation of approximately 0.3%. To address this issue,

a window filter is applied in a post-processing stage within the MCU. This filter effectively reduces the voltage dispersion to a much lower value of 0.06%.

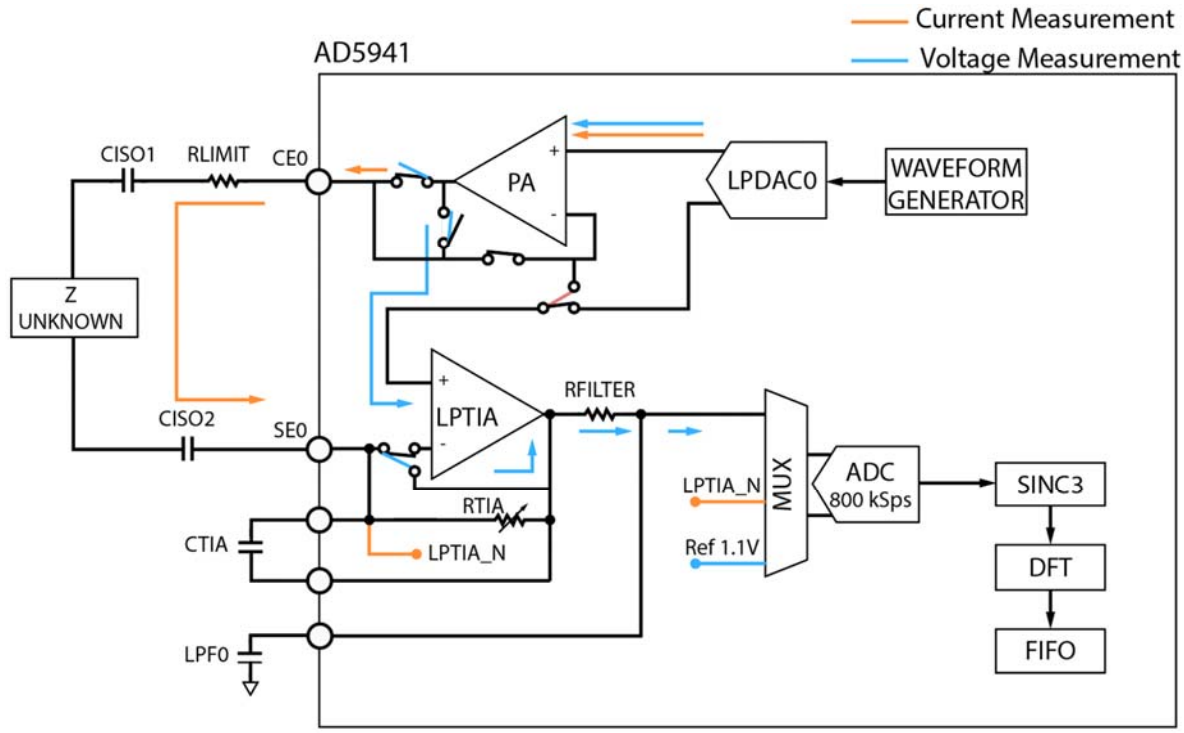

Fig. 4 Configuration of the connection matrix to measure voltage/current in AD-5941

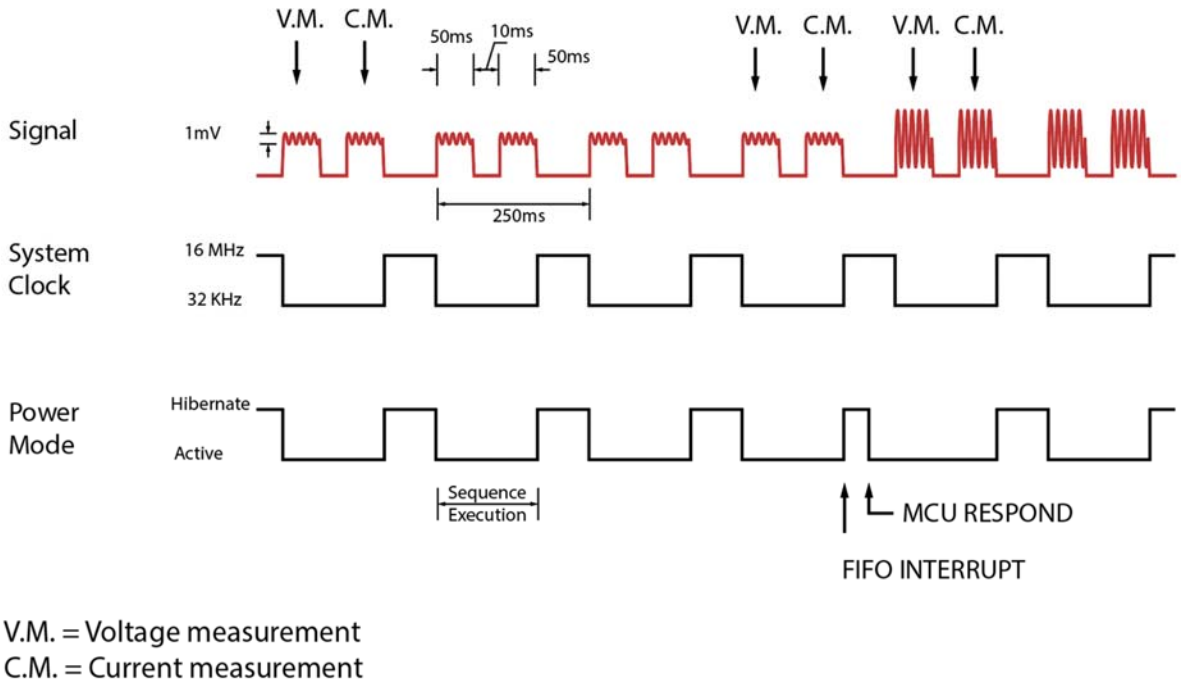

Fig. 5 Sequence of measurement using a constant current source

V. Experiment Design

To check the precision and accuracy of the implemented algorithm, a test bench was prepared. This test bench consisted of a set of resistors with values between 50 kΩ and 1000 kΩ. The objective of the test is to compare the performance of the algorithm proposed by Analog Devices with respect to the new proposed algorithm, using a constant current source.

To perform the comparison, a set of 200 samples was taken

for each resistance value. In (1), both algorithms were tested using a C_{ISO1} and C_{ISO2} value of 1 uF, and an R_{LIMIT} of 1 kΩ was used to enable measurement of low impedance values and demonstrate the feedback current mechanism to control the current under 10 uA. The objective of this test is to compare the changes in resistance and reactance as the value of the measured impedance increases.

VI. Results

After analyzing the set of samples, we calculate the variation coefficient using standard deviation and mean value (2), a summary of the data dispersion values for each test can be observed in Table I.

$$CV = \frac{\sigma_x}{|\bar{x}|} = \frac{\sqrt{\sum(x_i - \bar{x})^2}}{N \cdot |\bar{x}|} \quad (2)$$

A summary of the data dispersion values for each test can be observed in Table I. The first column shows all the resistor values used in the tests. In the second column, the dispersion value when using the constant voltage AC algorithm is shown (Analog Devices). Finally, the third column shows the dispersion value when using the algorithm proposed for a constant AC current source.

TABLE I
Dispersion Coefficient of Impedance

Resistance [kΩ]	Dispersion coefficient [%]	
	Voltage AC constant source	Current AC constant source
50	0.015	0.0027
100	0.0041	0.0046
270	0.0023	0.0037
560	0.0036	0.0069
1000	0.0081	0.0133

We can see that dispersion values increase in the worst case in a factor of 1.6 when employing the constant current algorithm for impedance measurement. As can be seen from Table I, the dispersion coefficient is larger when measured at constant current than when measured at constant voltage. However, the error committed undergoes a smaller variation at constant current than at constant voltage. This trend is confirmed by comparing the relative error associated with the different algorithms in Fig 6. The tendency of the constant voltage algorithm is to make an increasing error as the measured resistance value becomes smaller. However, the measurement at constant current shows a flatter error over the entire measurement range, becoming reduced by a factor of 10 for the lower resistor values. This phenomenon can be attributed to the use of a single RTIA value and the amplitude modulation of the voltage signal to achieve a constant current flow.

Also, when analyzing the variations in resistance and reactance, (see Fig. 7) it is observed that the constant current method exhibits lesser changes in reactance. The obtained values approach zero, which was expected since the experiment solely involved varying the electrical resistance. In other words, it is observed that the constant voltage source method and changes in RTIA values for current-to-voltage conversion in LPTIA can induce changes in reactance as the overall value of the LPTIA feedback impedance is changed.

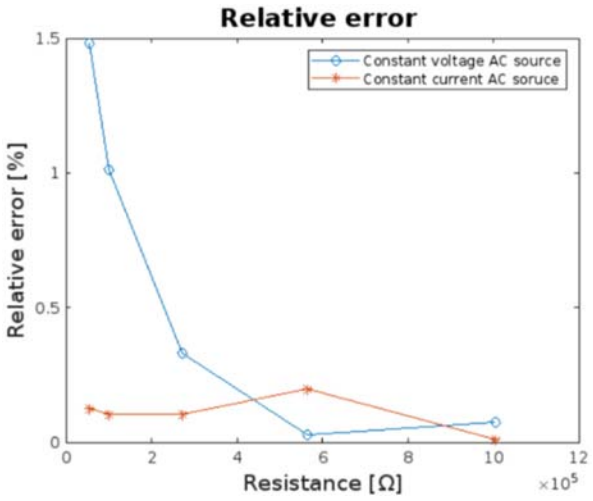

Fig. 6 Impedance measurement relative error

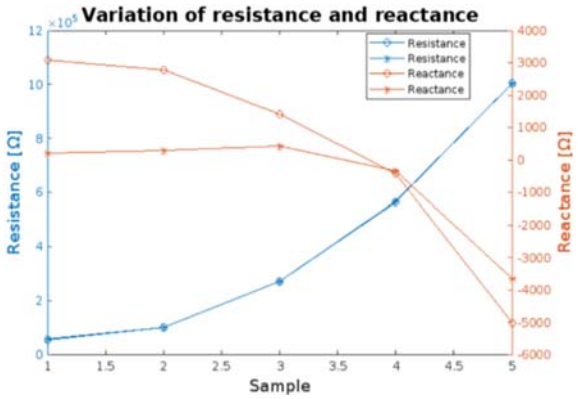

Fig. 7 Variation of resistance and reactance; in blue: constant voltage source, in orange: constant current source

VII. Conclusion

In conclusion, the proposed constant current algorithm shows a trade-off between data dispersion and accuracy. Although it generates a larger data dispersion, it also presents a lower relative error value, which ultimately improves the overall accuracy of the system. At the lower end of the measurement range, the algorithm achieves a remarkable 10-fold improvement in accuracy, although at a sacrifice of precision by a factor of 1.6. As a result, the system provides more accurate and reliable impedance values.

The use of an algorithm that allows the AD-5941 to be used as a constant current source is of great interest. This algorithm generates minimal alterations in the reactance values during impedance measurements, which can significantly improve the study of EDA. On the other hand, it ensures that changes in reactance are largely the result of individual variations and are not caused by the specific measurement system.

Acknowledgment

This work is part of the project Technological Ecosystem for

the MOod Recognition in cardiac rehabilitation patients (TEMOR), TED2021-130374B-C22, funded by MCIN/AEI/ 10.13039/501100011033 and by European Union NextGenerationEU/PRTR. Work is partly funded by the Aragonese Government (Group T60_23R).

REFERENCES

[1] C. Civilotti et al., "State of Mind Assessment in Relation to Adult Attachment and Text Analysis of Adult Attachment Interviews in a Sample of Patients with Anorexia Nervosa," European Journal of Investigation in Health, Psychology and Education, vol. 12, no. 12, Art. no. 12, Dec. 2022, doi: 10.3390/ejihpe12120124.

[2] S.-E. Jung et al., "The Effectiveness and Safety of Mind-Body Modalities for Mental Health of Nurses in Hospital Setting: A Systematic Review," International Journal of Environmental Research and Public Health, vol. 18, no. 16, Art. no. 16, Jan. 2021, doi: 10.3390/ijerph18168855.

[3] P. F. Berrocal and R. Cabello, "La inteligencia emocional como fundamento de la educación emocional," 2021.

[4] H. N. Parikh, H. N. Pandya, J. A. Savaliya, and B. H. Pithadiya, "Electrodermal Activity (EDA) and body temperature Monitoring system for patients with psychological disorder," J. Phys.: Conf. Ser., vol. 2007, no. 1, p. 012002, Aug. 2021, doi: 10.1088/1742-6596/2007/1/012002.

[5] A. Affanni, A. Piras, R. Rinaldo, and P. Zontone, "Dual channel Electrodermal activity sensor for motion artifact removal in car drivers' stress detection," in 2019 IEEE Sensors Applications Symposium (SAS), Mar. 2019, pp. 1–6. doi: 10.1109/SAS.2019.8706023.

[6] A. S. Anusha, S. P. Preejith, T. J. Akl, and M. Sivaprakasam, "Electrodermal activity based autonomic sleep staging using wrist wearable," Biomedical Signal Processing and Control, vol. 75, p. 103562, May 2022, doi: 10.1016/j.bspc.2022.103562.

[7] S. Sugimine, S. Saito, and T. Takazawa, "Normalized skin conductance level could differentiate physical pain stimuli from other sympathetic stimuli," Sci Rep, vol. 10, p. 10950, Jul. 2020, doi: 10.1038/s41598-020-67936-0.

[8] W. Boucsein, Electrodermal Activity. Boston, MA: Springer US, 2012. doi: 10.1007/978-1-4614-1126-0.

[9] J. G. Webster and A. J. Nimunkar, Medical Instrumentation: Application and Design. John Wiley & Sons, 2020.

[10] M. S. Mahmud, H. Fang, and H. Wang, "An Integrated Wearable Sensor for Unobtrusive Continuous Measurement of Autonomic Nervous System," IEEE Internet of Things Journal, vol. 6, no. 1, pp. 1104–1113, Feb. 2019, doi: 10.1109/JIOT.2018.2868235.

[11] A. Joglekar, G. Bhandari, and R. Sundaresan, "ESD wrist strap-based EDA sensor cum ESD strap integrity monitor," in IECON 2021 – 47th Annual Conference of the IEEE Industrial Electronics Society, Oct. 2021, pp. 1–6. doi: 10.1109/IECON48115.2021.9589358.

[12] J. Kim, S. Kwon, S. Seo, and K. Park, "Highly wearable galvanic skin response sensor using flexible and conductive polymer foam," in 2014 36th Annual International Conference of the IEEE Engineering in Medicine and Biology Society, Aug. 2014, pp. 6631–6634. doi: 10.1109/EMBC.2014.6945148.

[13] M.-Z. Poh, N. C. Swenson, and R. W. Picard, "A Wearable Sensor for Unobtrusive, Long-Term Assessment of Electrodermal Activity," IEEE Transactions on Biomedical Engineering, vol. 57, no. 5, pp. 1243–1252, May 2010, doi: 10.1109/TBME.2009.2038487.

[14] M. F. Canabal, J. A. Miranda, J. M. Lanza-Gutiérrez, A. I. Pérez Garcilópez, and C. López-Ongil, "Electrodermal Activity Smart Sensor Integration in a Wearable Affective Computing System," in 2020 XXXV Conference on Design of Circuits and Integrated Systems (DCIS), Nov. 2020, pp. 1–6. doi: 10.1109/DCIS51330.2020.9268662.

[15] H. F. Posada-Quintero and K. H. Chon, "Innovations in Electrodermal Activity Data Collection and Signal Processing: A Systematic Review," Sensors, vol. 20, no. 2, Art. no. 2, Jan. 2020, doi: 10.3390/s20020479.

[16] A. S. Anusha, S. P. Preejith, T. J. Akl, J. Joseph, and M. Sivaprakasam, "Dry Electrode Optimization for Wrist-based Electrodermal Activity Monitoring," in 2018 IEEE International Symposium on Medical Measurements and Applications (MeMeA), Jun. 2018, pp. 1–6. doi: 10.1109/MeMeA.2018.8438595.

[17] "UNE-EN 60601-1:2008 Equipos electromédicos. Parte 1: Requisito..." Accessed: Jun. 26, 2023. (Online). Available: https://www.une.org/encuentra-tu-norma/busca-tu-norma/norma?c=N0041083

[18] "AD5941 Datasheet and Product Info | Analog Devices." Accessed: Jun. 24, 2023. (Online). Available: https://www.analog.com/en/products/ad5941.html#product-overview